

Fractal Weyl laws for amplified states in \mathcal{PT} -symmetric resonators

Christopher Birchall and Henning Schomerus

Department of Physics, Lancaster University, Lancaster, LA1 4YB, United Kingdom

(Dated: November 14, 2021)

We find that in nonhermitian \mathcal{PT} -symmetric systems (as realized in resonators with balanced absorption and amplification), a mechanism based on quantum-to-classical correspondence reduces the occurrence of strongly amplified states. The reduction arises from semiclassically emerging hierarchical phase-space structures that are associated with the coupling of the amplifying and absorbing regions (forward and backward-trapped sets and their complements), and amounts to a generalization of the fractal Weyl law, earlier proposed for ballistically open systems. In the context of the recently introduced class of \mathcal{PT} -symmetric laser-absorbers, this phenomenon reduces the number of states participating in the mode competition.

PACS numbers: 42.55.-f, 03.65.-w, 05.45.Mt, 42.25.-p

Nonhermitian systems which can still possess a real spectrum have been realized very recently in optical [1, 2] electronic [3] and microwave [4] settings. These experiments utilize the concept of \mathcal{PT} symmetry [5, 6]—when an amplifying system is coupled symmetrically to an absorbing system, this can result in a precise balance of loss and gain for individual modes, which then have a real energy (the time reversal operation \mathcal{T} converts loss into gain and vice versa, while the parity operation \mathcal{P} interchanges the amplifying and absorbing parts of the system). For small absorption and amplification rates μ , this balance is robust, but if these rates are too large, pairs of real eigenenergies bifurcate into complex-conjugate pairs. This phenomenon is known as spontaneous \mathcal{PT} -symmetry breaking and leads to a range of remarkable switching effects [1, 2, 6–9]. In particular, \mathcal{PT} -symmetric optical resonators have been predicted to form a new class of lasers [10–12], which show an additional spectral peculiarity: lasing modes are degenerate with perfectly absorbing modes [11–13]. In the setting of these lasers, the focus shifts to the most strongly amplified modes, as these are best placed to overcome external losses, win the mode competition, and thus determine the laser threshold and radiation characteristics.

Here we report that the most strongly amplified modes in these \mathcal{PT} -symmetric resonators show the hallmarks of yet another distinctive spectral feature—a *fractal Weyl law*, by which the number of these modes is systematically reduced when the resonator dimensions are scaled up to become much larger than the wave length (the semiclassical limit, corresponding to an effective Planck’s constant $\hbar \ll 1$). Fractal Weyl laws have been originally established for passive leaky systems with chaotic underlying classical dynamics, where long-living states are supported by a fractal repeller—the number of these states then scales as h^{d_H} , where $d_H < d$ is the fractal dimension of the repeller in the d -dimensional phase space [14–18]. In order to uncover the analogous effects in the \mathcal{PT} -symmetric setting, we establish a quantum-to-classical correspondence [18–20] of various components

of the spectrum to specific regions in the classical phase space, with phase-space volumes reflecting the proportions of these components in the spectrum. We find that the strongly amplified states are supported by a hierarchical structure associated with the coupling of the amplifying and absorbing regions (the backward-trapped set in the amplifying parts of the system, which forms part of the classical repeller). The increasing phase-space resolution in the semiclassical limit reveals the sparse fractal nature of the backward-trapped set and thus results in the reduction of the number of strongly amplified modes mentioned above.

Model for nonhermitian \mathcal{PT} -symmetric resonator dynamics.— A model of the dynamics of waves in a resonator which displays the required \mathcal{PT} symmetry can be set up as follows (see Fig. 1). We divide the Hilbert space into two subspaces L, R , each of dimension M , with the first subspace representing the absorbing region in a ‘left’ resonator and the second subspace representing the amplifying region in a ‘right’ resonator. In each resonator, the ballistic chaotic dynamics over a finite time interval $\Delta t \equiv 1$ is described by an $M \times M$ -dimensional unitary time-evolution operator $F_L = F$ and $F_R = [F^{-1}]^* = F^T$, respectively, where the stated relation between F_L and

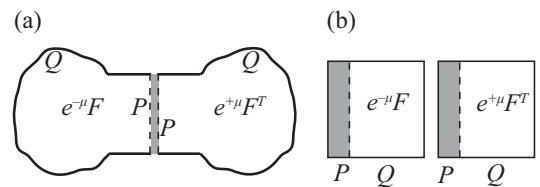


FIG. 1: (a) Sketch of a \mathcal{PT} -symmetric resonator, consisting of an absorbing resonator (left) coupled to an amplifying resonator (right). The unitary operator F describes the internal dynamics in each resonator, the factors $e^{\pm\mu}$ model amplification and absorption, and the projectors P (onto the interface) and Q (onto the walls) describe the coupling, altogether resulting in the quantum map (2). (b) The Hilbert space (and the classical phase space) divides into an absorbing and an amplifying part, coupled in a subspace (shaded gray).

F_R ensures \mathcal{PT} symmetry [10, 12]. In each time step, the wave amplitude in the absorbing region is reduced by a factor $\exp(-\mu)$, while in the amplifying region it is enhanced by $\exp(\mu)$. This breaks the unitarity of the time evolution, but because of the matching rates again respects \mathcal{PT} symmetry. Finally, the ballistic coupling between the subspaces is described by a coupling matrix

$$C = \begin{pmatrix} Q & -iP \\ -iP & Q \end{pmatrix}, \quad P = \text{diag}(\underbrace{1, \dots, 1}_N, \underbrace{0, \dots, 0}_{M-N}). \quad (1)$$

where P projects onto the interface between the two resonators (with N channels connecting the resonators), while $Q \equiv \mathbb{1}_M - P$ represents the projector onto the walls of each resonator.

With these specifications, the time evolution of the composed system can be written as

$$\mathcal{F} = \sqrt{C} \begin{pmatrix} e^{-\mu} F & 0 \\ 0 & e^{\mu} F^T \end{pmatrix} \sqrt{C}, \quad (2)$$

where we symmetrized the coupling by means of the unitary matrix $\sqrt{C} = \begin{pmatrix} 2^{-1/2}P + Q & -i2^{-1/2}P \\ -i2^{-1/2}P & 2^{-1/2}P + Q \end{pmatrix}$ which squares to C . The operator \mathcal{F} acts on $2M$ -dimensional vectors $\psi = \begin{pmatrix} \psi_L \\ \psi_R \end{pmatrix}$, with the M entries in ψ_L giving the wave amplitude in the absorbing subsystem, and the remaining M entries in ψ_R giving the wave amplitude in the amplifying subsystem.

The spectrum of the system is now obtained from the eigenvalue equation

$$\mathcal{F}\psi_n = \lambda_n\psi_n, \quad \lambda_n = \exp(-iE_n), \quad (3)$$

where $E_n = \varepsilon_n - i\Gamma_n/2$ are quasienergies. The \mathcal{PT} symmetry of the quantum map (2) is manifest by the relation

$$\mathcal{F} = \mathcal{P}[\mathcal{F}^{-1}]^*\mathcal{P}, \quad (4)$$

where the parity operator is of the explicit form $\mathcal{P} = \begin{pmatrix} 0 & \mathbb{1}_M \\ \mathbb{1}_M & 0 \end{pmatrix} = \mathbb{1}_M \otimes \sigma_x$ (thus, \mathcal{P} interchanges the amplitudes of the subsystems). The spectral properties associated with \mathcal{PT} symmetry are now embodied in the characteristic polynomial $s(\lambda) = \det(\mathcal{F} - \lambda)$, of degree $2M$. Due to \mathcal{PT} symmetry, this polynomial exhibits the mathematical property of *self-inversiveness* [21, 22]:

$$s(1/\lambda^*) = [\lambda^{-2M} s(\lambda)]^* s(0), \quad (5)$$

where $s(0) = \det \mathcal{F} = (\det F)^2$ is a unimodular complex number. The eigenvalues are the roots of the secular equation $s(\lambda) = 0$. For each eigenvalue λ_n , we are thus guaranteed to find the eigenvalue $\lambda_{\bar{n}} = [\lambda_n^{-1}]^*$. It is possible that $n = \bar{n}$; then $|\lambda_n| = 1$, which means that the quasienergy $E_n = i \ln \lambda_n$ is real. For $n \neq \bar{n}$, we obtain complex quasienergies, which thus still appear in pairs

($E_{\bar{n}} = E_n^*$). If $\mu = 0$, \mathcal{F} is unitary, and all quasienergies are real. In the semiclassical limit of large $M = h^{-1}$ and fixed classical coupling strength N/M , and with μ increasing from zero, one expects a quasi-monotonous increase of the fraction of complex energies.

Dynamical signatures of spontaneous \mathcal{PT} -symmetry breaking.— We now investigate how the transition from a real to a complex spectrum depends on the dynamics of the system. In the resonator setting, nonintegrable dynamics arise from resonator walls of a generic shape. In the quantum map (2), this can be modeled by choosing a suitable operator F for the internal dynamics. In an optical setting, the passive system is time-reversal invariant, which furthermore dictates $F = F^T$. We implement these features via a paradigm of wave dynamics with a nonintegrable classical limit, the kicked rotator [23, 24]. The time-evolution operator of this system is given by

$$F_{mm'} = (iM)^{-1/2} e^{\frac{i\pi}{M}(m-m')^2 - \frac{iMk}{4\pi} \left(\cos \frac{2\pi m}{M} + \cos \frac{2\pi m'}{M} \right)}, \quad (6)$$

where the kicking strength k controls the dynamics from classically integrable ($k = 0$) to globally chaotic ($k \gtrsim 7$); the classical map is $q' = q + p + (k/4\pi) \sin(2\pi q) \pmod{1}$, $p' = p + (k/4\pi)[\sin(2\pi q) + \sin(2\pi q')] \pmod{1}$. We focus on the chaotic cases with $k = 8$, fix the coupling of the absorbing and amplifying regions by setting the inverse average dwell time in the amplifying or absorbing regions (the Thouless energy) to $E_T = N/M = 1/5$, and analyze the spectrum (obtained by diagonalizing \mathcal{F}) as a function of the amplification rate μ and the system size M .

We start with the distribution of decay rates, encoded in $\text{Im } E$, where large positive values indicate strong amplification and large negative values indicate strong decay. The left panels in Fig. 2 show histograms of this quantity for three representative values of μ . For comparison, the right panels show results from random-matrix theory, with F taken from the circular orthogonal ensemble [25]. All histograms are symmetric because complex energies appear in conjugate pairs, as imposed by \mathcal{PT} symmetry. Furthermore, the histograms display a sharp peak at $\text{Im } E = 0$, which arises from the states with real energies. This peak decreases with increasing systems size M , indicating that the proportion of such states vanishes in the semiclassical limit. As regards to this peak, there is good correspondence between the dynamical system and random-matrix theory, which predicts that the spectrum essentially turns complex at $\mu_c = \sqrt{N}/M \ll E_T$ [26].

For $\mu = 0.5E_T$ (top panel), this agreement between both models also extends to finite values of $\text{Im } E$, even though some difference are noticeable. The differences become more marked as μ exceeds E_T (middle and bottom panels)—in particular, in comparison to random-matrix theory, the dynamical system possesses a significantly reduced number of strongly amplified states, with large $\text{Im } E$. The insets in the bottom panel focus on the

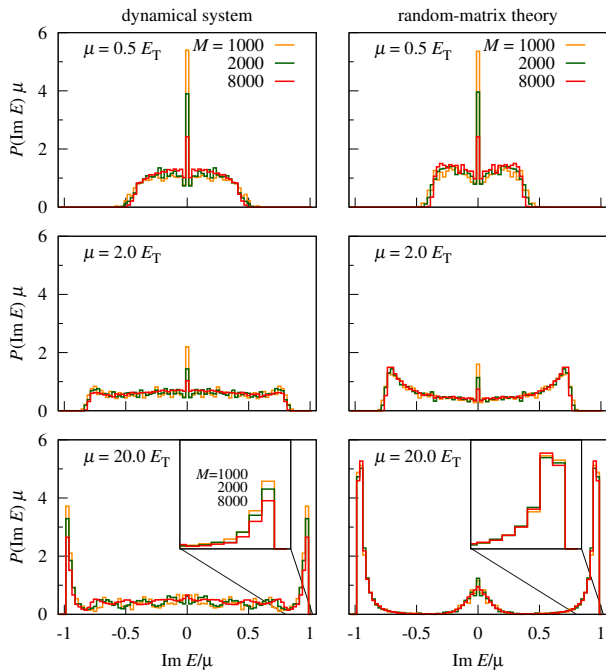


FIG. 2: (Color online) Distributions of $\text{Im} E$ in a \mathcal{PT} -symmetric resonator with Thouless energy $E_T \equiv N/M = 1/5$ for various amplification rates μ and system sizes M , numerically obtained from Eqs. (2), (3) with internal dynamics modeled via the kicked rotator (6) with $k = 8$ (left) and via random-matrix theory (right). Significant differences occur when μ exceeds E_T . For the kicked rotator, the proportion of strongly amplified states decreases systematically with increasing M , as highlighted in the inset of the bottom panel.

peak associated with these states. In the dynamical system, their proportion decreases systematically as M increases, while in random-matrix theory their proportion does not change.

In order to quantify this systematic reduction we consider the fraction of states with $\text{Im} E > \mu/2$, denoted as $f_>$ and plotted as a function of μ in the left panel of Fig. 3. In random-matrix theory, this curve becomes independent of M when M is large. For the dynamical system, however, $f_>(\mu)$ drops as M increases, even at the largest computationally accessible system sizes ($M = 8000$, corresponding to a matrix dimension 16 000 for \mathcal{F}). As shown in the right panel this drop follows a power-law $f_>(\mu) \propto M^{-a}$, with $a = 0.102(9)$ ($\mu = E_T$), $a = 0.079(6)$ ($\mu = 2E_T$), and $a = 0.069(8)$ ($\mu = 2E_T$). This data confirms that deviations from random-matrix theory set in as μ exceeds E_T . That the deviations increase with M points to a semiclassical origin, which we identify next.

Following previous investigations of general non-hermitian systems that addressed the issue of state nonorthogonality [18, 19], we identify the semiclassical support of the eigenstates in different components of the spectrum by constructing an orthonormal basis ϕ_n of the subspace spanned by the states, and then summing

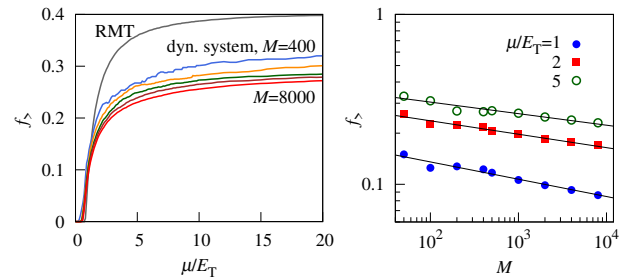


FIG. 3: (Color online) Left panel: Fraction $f_>(\mu)$ of strongly amplified states with $\text{Im} E > \mu/2$, as a function of μ . The random-matrix curve (RMT) is evaluated at $M = 8000$, while the curves for the dynamical system (specified in Fig. 2) correspond to $M = 400, 1000, 2000, 4000$ and 8000 . The double-logarithmic plot in the right panel demonstrates power-law scaling $f_> \propto M^{-a}$ at fixed $\mu = E_T$ ($a = 0.102(9)$), $2E_T$ ($a = 0.079(6)$), and $5E_T$ ($a = 0.069(8)$).

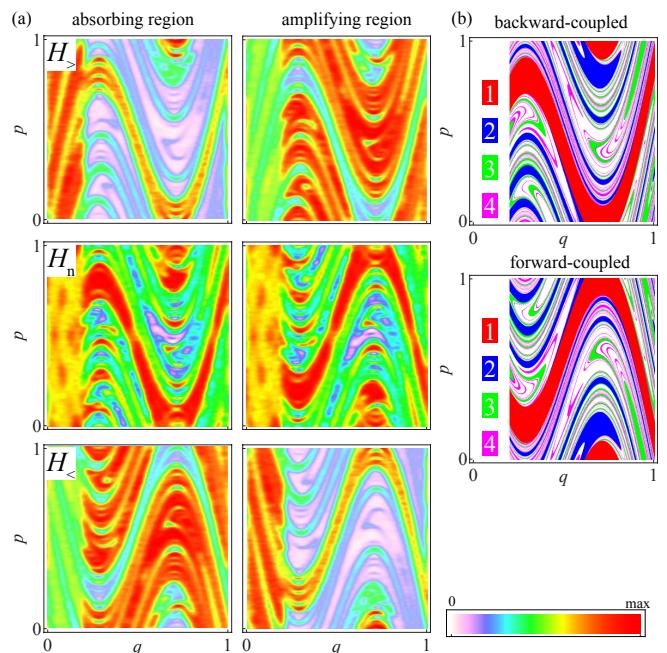


FIG. 4: (Color online) (a) Husimi phase-space distributions of the support of strongly amplified states ($\text{Im} E > \mu/2$, $H_>$), ‘neutral’ states ($|\text{Im} E| < \mu/2$, H_n), and strongly decaying states ($\text{Im} E < -\mu/2$, $H_<$), obtained for the kicked-rotator model of a \mathcal{PT} -symmetric resonator with $k = 8$, $M = 1000$, $E_T = 1/5$, $\mu = 2E_T$. (b) Classical phase-space regions which are coupled to the interface by 1–4 steps, backwards in time (top panel) or forwards in time (bottom panel).

the Husimi phase-space representations $H(q, p)$ of the basis states, defined by the squared overlap $|\langle q, p | \phi_n \rangle|^2$ with minimal-uncertainty wavepackets centered at phase space position (q, p) . Figure 4(a) shows these distributions for $\mu = 2E_T$ and $M = 1000$. The top panel depicts the support $H_>$ of the states with $\text{Im} E > \mu/2$, which

contribute to the quantity $f_>(\mu)$ discussed above. The middle panel shows the support H_n of ‘neutral’ states with $|\text{Im} E| < \mu/2$, while the bottom panel shows the support $H_<$ of quickly decaying states with $\text{Im} E < -\mu/2$. The distributions $H_>$ and $H_<$ are related by \mathcal{PT} symmetry, which interchanges the absorbing and amplifying regions and maps the momentum $p \rightarrow -p$; H_n is invariant under these operations.

The systematic structures observed in these distributions have a specific classical dynamical interpretation, which follows from the plots shown in panel (b) of Fig. 4. The top panel in (b) shows *backward-coupled regions* which are populated from the interface after 1 – 4 times steps of the classical dynamics. Including higher iterations, this hierarchical structure defines the complement of the *backward-trapped set*, a fractal which contains all points whose backwards-in-time dynamics does not meet the interface. The lower panel in (b) shows the analogous *forward-coupled regions*, which propagate towards the interface and define the complement of the *forward-trapped set* (the time reverse of the backward-trapped set).

Coming back to panel (a), we now recognize that in the amplifying part of phase space, the strongly amplified states mainly populate the backward-trapped set, and thus concentrated in regions of maximal dwell time. In the absorbing part of the system, these states are supported by the backward-coupled regions, which signifies minimal dwell time in this part of the system. A power-law suppression $\propto M^{-a}$ of the number of these states now follows from the fractal nature of the backward-trapped set, which is resolved in more detail in the semiclassical limit (according to the shrinking size $1/M$ of a Planck cell in phase space). The relevant fractal repeller dimension can then be estimated from the data in Fig. 3 as $d_H = 2 - a$ (the precise definition of this dimension in the context of fractal Weyl laws is an open problem). For larger values of μ , $f_>$ picks up larger parts of the bulk of the distribution $P(\text{Im} E)$, thus reducing the slope and overestimating d_H . We note that there are quantum fluctuations as a function of M , and classical finite-size effects as the dwell time $E_T^{-1} = 5$ is not asymptotically large. For the strongly decaying states, the same argumentation carries over to the forward-trapped set. Furthermore, the neutral states are supported by the backward-coupled regions in the amplifying part, and the forward-coupled regions in the absorbing parts, thus resulting in an (approximate) balance of amplification and absorption which becomes exact for states with $\text{Im} E = 0$.

In conclusion, the spectral properties of \mathcal{PT} -symmetric systems with complex wave dynamics show clear signatures of the underlying classical dynamics, and in particular, the details of the coupling between amplifying and absorbing regions. Strongly amplified states are supported by the backward-trapped set in the amplifying region, while states with real or almost real energies are supported by regions that are well connected to both the

amplifying and the absorbing parts of the system. The fractal nature of the backward-trapped set results in a systematic reduction of strongly amplified states, which becomes more marked for large system sizes, and follows the characteristic power-law dependence of a fractal Weyl law (earlier predicted only for leaky systems with ballistic openings).

The experimental observation of the ordinary fractal Weyl law has proven a challenge as it addresses decaying quasi-bound states. In contrast, the fractal Weyl law uncovered here applies to amplified and possibly lasing states. This phenomenon should generally affect the properties of the discussed class of \mathcal{PT} -symmetric laser-absorbers, where the strongly amplified states dominate the mode competition. However, conceptually our findings also carry over to other classes of nonhermitian dynamical systems, including passive realizations of \mathcal{PT} symmetry [1, 4], as well as systems which combine amplification and absorption in a non-symmetrical fashion [27]. The main requirements are multiple scattering on long time scales and ballistic wave propagation on short time scales, including a ballistic coupling between the regions of different amplification or absorption rate; the most amplified (or least decaying) states are then semiclassically supported by the backward-trapped set in the most amplifying (or least absorbing) regions.

-
- [1] A. Guo, G. J. Salamo, D. Duchesne, R. Morandotti, M. Volatier-Ravat, V. Aimez, G. A. Siviloglou, and D. N. Christodoulides, *Phys. Rev. Lett.* **103**, 093902 (2009).
 - [2] C. E. Rüter, K. G. Makris, R. El-Ganainy, D. N. Christodoulides, M. Segev, and D. Kip, *Nature Phys.* **6**, 192 (2010).
 - [3] J. Schindler, A. Li, M. C. Zheng, F. M. Ellis, and T. Kottos, *Phys. Rev. A* **84**, 040101 (2011).
 - [4] S. Bittner, B. Dietz, U. Günther, H. L. Harney, M. Miski-Oglu, A. Richter, and F. Schäfer, *Phys. Rev. Lett.* **108**, 024101 (2012).
 - [5] C. M. Bender and S. Boettcher, *Phys. Rev. Lett.* **80**, 5243 (1998).
 - [6] R. El-Ganainy, K. G. Makris, D. N. Christodoulides, and Z. H. Musslimani, *Opt. Lett.* **32**, 2632 (2007); K. G. Makris, R. El-Ganainy, D. N. Christodoulides, and Z. H. Musslimani, *Phys. Rev. Lett.* **100**, 103904 (2008); Z. H. Musslimani, K. G. Makris, R. El-Ganainy, and D. N. Christodoulides, *ibid.* **100**, 030402 (2008).
 - [7] S. Longhi, *Phys. Rev. Lett.* **103**, 123601 (2009).
 - [8] M. C. Zheng, D. N. Christodoulides, R. Fleischmann, and T. Kottos, *Phys. Rev. A* **82**, 010103 (2010).
 - [9] A. A. Sukhorukov, Z. Xu, and Y. S. Kivshar, *Phys. Rev. A* **82**, 043818 (2010).
 - [10] H. Schomerus, *Phys. Rev. Lett.* **104**, 233601 (2010); G. Yoo, H.-S. Sim, and H. Schomerus, *Phys. Rev. A* **84**, 063833 (2011).
 - [11] S. Longhi, *Phys. Rev. A* **82**, 031801(R) (2010).
 - [12] Y. D. Chong, L. Ge, and A. D. Stone, *Phys. Rev. Lett.* **106**, 093902 (2011); L. Ge, Y. D. Chong, and A. D. Stone, *Phys. Rev. A* **85**, 023802 (2012).
 - [13] Y. D. Chong, L. Ge, H. Cao, and A. D. Stone, *Phys. Rev.*

- Lett. **105**, 053901 (2010); W. Wan, Y. Chong, L. Ge, H. Noh, A. D. Stone, and H. Cao, *Science* **331**, 889 (2011).
- [14] J. Sjöstrand, *Duke Math. J.* **60**, 1 (1990).
- [15] M. Zworski, *Not. Am. Math. Soc.* **46**, 319 (1999); W. T. Lu, S. Sridhar, and M. Zworski, *Phys. Rev. Lett.* **91**, 154101 (2003); S. Nonnenmacher and M. Zworski, *J. Phys. A* **38**, 10683 (2005).
- [16] H. Schomerus and J. Tworzydło, *Phys. Rev. Lett.* **93**, 154102 (2004).
- [17] J. P. Keating, M. Novaes, S. D. Prado, and M. Sieber, *Phys. Rev. Lett.* **97**, 150406 (2006).
- [18] L. Ermann, G. G. Carlo, and M. Saraceno, *Phys. Rev. Lett.* **103**, 054102 (2009).
- [19] M. Kopp and H. Schomerus, *Phys. Rev. E* **81**, 026208 (2010).
- [20] E.-M. Graefe, M. Höning, and H. J. Korsch, *J. Phys. A: Math. Theor.* **43**, 075306 (2010); E.-M. Graefe and R. Schubert, *Phys. Rev. A* **83**, 060101(R) (2011).
- [21] E. Bogomolny, O. Bohigas, and P. Leboeuf, *Phys. Rev. Lett.* **68**, 2726 (1992).
- [22] F. Haake, M. Kuś, H.-J. Sommers, H. Schomerus, and K. Życzkowski, *J. Phys. A* **29**, 3641 (1996).
- [23] F. M. Izrailev, *Phys. Rep.* **196**, 299 (1990).
- [24] For a related waveguide model see C. T. West, T. Kottos, and T. Prosen, *Phys. Rev. Lett.* **104**, 054102 (2010).
- [25] M. L. Mehta, *Random Matrices*, 3rd ed. (Elsevier, New York, 2004).
- [26] H. Schomerus, *Phys. Rev. A* **83**, 030101(R) (2011).
- [27] L. Ge, Y. D. Chong, S. Rotter, H. E. Türeci, and A. D. Stone, *Phys. Rev. A* **84**, 023820 (2011).